Research Square

Preprints are preliminary reports that have not undergone peer review.
They should not be considered conclusive, used to inform clinical practice,
or referenced by the media as validated information.

Physiological and metabolic responses of dill to nano-silica and nano-zinc under drought stress: implications for yield and essential oil quality

Hanan Khalaf Anazi
University College of Duba, University of Tabuk
Taghreed S. Alnusaire
Jouf University
Khulud S. Albalawi
University College of Duba, University of Tabuk
Siham M. AL-Balawi
University College of Duba, University of Tabuk
Ibtisam A. M. Alghabban
University College of Duba, University of Tabuk
Almaghamsi Afaf
University of Jeddah
Suliman M .S. Alghanem
Qassim University
Wasimah AlShammari
University of Hail
Dalal Alenizi
University of Hail
Hailah M. Almohaimeed
Princess Nourah bint Abdulrahman, University
Mona H. Soliman
monahsh1@gamil.com

College of Science in Yanbu, Taibah University
Marwa A Fakhr
Fayoum University

Research Article

Keywords: Drought stress, Nano-particles, Essential oil composition, Oxidative stress tolerance

Posted Date: December 26th, 2025

DOI: https://doi.org/10.21203/rs.3.rs-8018417/v1

License: This work is licensed under a Creative Commons Attribution 4.0 International License. Read Full License

Additional Declarations: No competing interests reported.

Version of Record: A version of this preprint was published at BMC Plant Biology on February 20th, 2026. See the published version at https://doi.org/10.1186/s12870-026-08321-3.

Abstract

Drought stress severely limits the productivity of medicinal and aromatic plants by disrupting physiological processes and altering secondary metabolism. This study investigated the potential of nano-silica (Si) and nano-zinc (Zn) to improve drought resilience and essential oil quality in dill (*Anethum graveolens* L.) across two growing seasons (2023–2024). The experiment was conducted in a split-plot design with two irrigation regimes (well-watered and drought stress at flowering stage) and six nano-fertilizer treatments (control, Si25, Si100, Zn25, Zn50, Zn100). Nanoparticles were synthesized via sol–gel (Si) and precipitation (Zn) methods and characterized using DLS, zeta potential, SEM, XRD, and FTIR analyses. Results showed that drought stress significantly reduced chlorophyll retention, photosynthetic efficiency, root biomass, and seed yield, while increasing oxidative damage indicators such as malondialdehyde (MDA), electrolyte leakage (EL), hydrogen peroxide (H_2O_2), and superoxide radicals ($O_2^{\bullet -}$). Application of nano-silica and nano-zinc markedly mitigated these negative effects, with higher doses (Si100 and Zn100) being most effective. Treated plants exhibited enhanced SPAD index, photosynthetic rate, and root growth, alongside elevated proline accumulation and reduced oxidative stress markers, thereby preserving membrane stability and sustaining photosynthetic function. These improvements translated into significantly higher seed yield and harvest index under both irrigation regimes. In addition to primary physiology, nano-fertilizer treatments reprogrammed secondary metabolism, enhancing the accumulation of key monoterpenes (α-pinene, limonene, dill ether) and phenylpropanoids (carvacrol, apiole) in essential oil profiles, particularly under drought stress. The cumulative effects were more pronounced in the second year, highlighting stable and seasonally reinforced benefits of nano-fertilizer application. Overall, this study demonstrates that nano-silica and nano-zinc act through multifaceted mechanisms—including structural reinforcement, osmotic adjustment, antioxidant activation, and metabolic reprogramming—to alleviate drought-induced damage while improving yield and essential oil quality in dill. These findings underscore the dual agronomic and industrial value of nano-fertilizers as sustainable tools for enhancing resilience and product quality in climate-sensitive crops.

Introduction

Drought stress is one of the most serious environmental constraints limiting the productivity of crops worldwide. Water deficit disrupts multiple physiological and biochemical processes, including photosynthetic efficiency, nutrient uptake, osmotic balance, and membrane stability, ultimately reducing yield and quality [1–3]. In aromatic and medicinal plants, drought stress not only diminishes biomass accumulation but also alters secondary metabolism, affecting essential oil yield and composition [4, 5]. With the increasing frequency of drought events due to climate change, there is an urgent need to develop effective strategies that enhance plant resilience while maintaining both agronomic and industrially important traits.

Nano-fertilizers have emerged as promising tools in sustainable agriculture owing to their high surface area, reactivity, and controlled nutrient release. Unlike conventional fertilizers, nano-based inputs can penetrate plant tissues more efficiently, modulate physiological processes, and enhance stress tolerance [6]. Among these, nano-silica (Si) and nano-zinc (Zn) are of particular interest. Silicon is recognized as a beneficial element that strengthens plant structural defenses, reduces transpirational water loss, and improves antioxidant activity [7]. Although not considered essential for all plants, silicon has been shown to alleviate the detrimental effects of drought by stabilizing membranes, enhancing chlorophyll retention, and improving root water uptake [1]. Zinc, on the other hand, is an essential micronutrient that plays critical roles in enzyme activation, protein synthesis, chlorophyll biosynthesis, and reproductive development [8]. Zinc deficiency is common under drought conditions, leading to impaired photosynthesis, reduced seed set, and decreased crop productivity.

The integration of nano-silica and nano-zinc provides a dual mechanism of action: silicon contributes structural and physiological protection, while zinc ensures enzymatic and metabolic regulation. Recent studies have demonstrated that nanostructured forms of these elements are more efficient than their bulk counterparts in enhancing photosynthesis, improving water relations, and mitigating oxidative damage under stress. However, their combined effects on aromatic plants, particularly in relation to both yield and essential oil composition, remain poorly understood.

Dill (*Anethum graveolens* L.) is a widely cultivated medicinal and culinary herb valued for its essential oil, which contains bioactive compounds such as carvone, limonene, and apiole with applications in the pharmaceutical, flavoring, and food industries. The quantity and quality of dill essential oil are highly sensitive to environmental stresses, especially drought [9]. Enhancing drought tolerance in dill while simultaneously improving essential oil yield and composition would therefore have both agronomic and economic significance [10].

Given this background, the present study was undertaken to investigate the effects of nano-silica and nano-zinc on the physiological, biochemical, and metabolic responses of dill under irrigation and drought stress conditions over two growing seasons, with specific objectives to: (i) evaluate their influence on chlorophyll retention (SPAD index), photosynthetic traits, root biomass, seed yield, and harvest index; (ii) assess biochemical markers of stress tolerance, including proline, malondialdehyde (MDA), electrolyte leakage (EL), hydrogen peroxide (H_2O_2), and superoxide radicals ($O_2^{\bullet -}$); and (iii) characterize changes in essential oil composition. The novelty of this work lies in its integrative, multi-level approach that links primary physiology with secondary metabolism, providing the first evidence that nano-silica and nano-zinc not only alleviate drought-induced losses in growth and photosynthesis but also reprogram essential oil biosynthesis in dill. The importance of the study is underscored by its dual relevance: offering a sustainable agronomic strategy to improve drought resilience in a climate-sensitive crop, and demonstrating an industrial pathway to enhance essential oil yield and quality, thereby adding economic value to medicinal and aromatic plant production.

Materials and Methods

Plant Material and Growth Conditions

Dill (*Anethum graveolens* L.) seeds were obtained from an Agricultural Research Centre, Ministry of Agriculture, Giza, Egypt. Prior to sowing, seeds were surface-sterilized with 2% sodium hypochlorite for 5 min, rinsed thoroughly with distilled water, and air-dried. Plants were grown under natural field conditions during the 2023 and 2024 seasons at the Department of Biology, College of Science in Yanbu, Taibah University, Saudi Arabia during 2023 and 2024 with average day/night temperatures of 25/18°C, relative humidity of 60–70%, and photoperiod of 14 h light/10 h dark. Standard agronomic practices were followed to maintain crop growth. he physicochemical properties of the experimental soil for the two seasons are presented in Table 1.

Experimental Design and Treatments

The experiment was conducted in a split-plot design, with irrigation regime as the main plot factor and nano-fertilizer treatments as the subplot factor. Two irrigation regimes were applied: well-watered (80–85% field capacity throughout the growing period) and drought stress, imposed at the flowering stage by withholding irrigation until soil moisture declined to approximately 30% of field capacity. The subplot treatments consisted of six levels: control (no nano-fertilizer), Si25 (25 mg L^{-1} nano-silica), Si100 (100 mg L^{-1} nano-silica), Zn25 (25 mg L^{-1} nano-zinc), Zn50 (50 mg L^{-1} nano-zinc), and Zn100 (100 mg L^{-1} nano-zinc). Each treatment was replicated three times. The nano-silica and nano-zinc particles were dispersed in distilled water using ultrasonication and applied as foliar sprays at 30 and 50 days after sowing.

Synthesis and Characterization of Nanoparticles

Synthesis of Nano-Silica

Nano-silica particles were synthesized following a sol–gel method with slight modifications (referenced protocol). Briefly, tetraethyl orthosilicate (TEOS) was used as the silica precursor and hydrolyzed in an ethanol–water medium under constant stirring. Ammonia solution was added dropwise as a catalyst to initiate condensation and particle growth. The reaction mixture was maintained at room temperature for 12 h to allow complete gelation, followed by centrifugation to collect the nanoparticles. The obtained precipitate was washed several times with deionized water and ethanol to remove unreacted residues, and then dried at 80°C. Finally, the dried material was calcined at 550°C for 4 h to enhance structural stability and remove organic remnants.

Synthesis of Nano-Zinc

Nano-zinc particles were prepared by chemical precipitation. Zinc sulfate heptahydrate ($ZnSO_4 \cdot 7H_2O$) was dissolved in deionized water and stirred continuously. Sodium hydroxide solution (0.2 M) was added dropwise to the zinc precursor under vigorous stirring until the pH reached 11, resulting in the formation of a white precipitate of zinc hydroxide. The suspension was aged for 24 h at room temperature, followed by centrifugation and repeated washing with deionized water and ethanol to remove impurities. The obtained precipitate was dried at 80°C and subsequently calcined at 400°C for 3 h to obtain zinc oxide nanoparticles.

Characterization of Nanoparticles

The synthesized nanoparticles were characterized using multiple techniques. Particle morphology and surface features were examined by scanning electron microscopy (SEM; MIRA3 TESCAN) operated at 30 kV with backscattered electron (BSE) and secondary electron (SE) detectors. Particle size distribution and hydrodynamic diameter were determined using dynamic light scattering (DLS; Malvern Zetasizer Nano). Surface charge and colloidal stability were evaluated by zeta potential analysis. The crystalline structure of the nanoparticles was analyzed by X-ray diffraction (XRD; Bruker D8 Advance, Cu-Kα radiation, λ = 1.5406 Å), and functional groups were identified using Fourier-transform infrared spectroscopy (FTIR; PerkinElmer Spectrum 100, 4000–400 cm^{-1} range).

Physiological Parameters

SPAD Index

Chlorophyll content was estimated nondestructively using a SPAD-502 Plus chlorophyll meter (Konica Minolta, Japan). Measurements were taken from the uppermost fully expanded leaves at 60 days after sowing. Three readings per leaf were recorded from five randomly selected plants per replicate and averaged.

Root Dry Weight

Plants were carefully uprooted at harvest, and roots were washed with running water. Samples were oven-dried at 70°C for 72 h until constant weight was achieved. Dry weight was expressed in grams per plant.

Seed Yield and Harvest Index

Seed yield was determined by harvesting mature umbels at physiological maturity and drying seeds to 12% moisture content. Yield was expressed as g $plant^{-1}$. Harvest index (HI) was calculated as the ratio of seed yield to total aboveground biomass × 100.

Photosynthetic Parameters

Gas exchange measurements were conducted using a portable infrared gas analyzer (LI-6400XT, LI-COR, USA) on fully expanded top leaves between 09:00 and 11:00 h on clear days. Parameters recorded included net photosynthetic rate (Pn, μmol CO_2 m^{-2} s^{-1}), stomatal conductance (Gs, mol H_2O m^{-2} s^{-1}), transpiration rate (E, mmol H_2O m^{-2} s^{-1}), and intercellular CO_2 concentration (Ci, μmol mol^{-1}). Chamber conditions were maintained at 25°C, 380 ppm CO_2, and 1000 μmol m^{-2} s^{-1} photosynthetic photon flux density (PPFD).

Biochemical Parameters

Proline Content

Proline concentration was determined following the acid–ninhydrin method of Bates et al. (1973). Fresh leaf tissue (0.5 g) was homogenized in 3% sulfosalicylic acid, centrifuged at 10,000 × g for 10 min, and 2 mL of the supernatant was reacted with 2 mL glacial acetic acid and 2 mL ninhydrin reagent in a water bath (100°C, 1 h). The reaction was stopped in an ice bath, and the mixture was extracted with 4 mL toluene. Absorbance was read at 520 nm, and proline concentration was calculated using a standard curve [11].

Malondialdehyde (MDA)

Lipid peroxidation was assessed by measuring thiobarbituric acid-reactive substances (TBARS) as described by Heath and Packer (1968). Fresh leaf tissue (0.5 g) was homogenized in 5 mL 0.1% trichloroacetic acid (TCA), centrifuged at 12,000 × g for 15 min, and 2 mL of supernatant was mixed with 2 mL 0.5% thiobarbituric acid in 20% TCA. The mixture was heated at 95°C for 30 min, cooled on ice, and centrifuged again. Absorbance was recorded at 532 and 600 nm, and MDA concentration was calculated using an extinction coefficient of 155 mM^{-1} cm^{-1} [12].

Electrolyte Leakage (EL)

Membrane stability was assessed by the electrolyte leakage method [13]. Leaf discs (0.5 g) were rinsed in distilled water and incubated in 25 mL of deionized water at 25°C for 24 h. Initial conductivity (C1) was measured using a conductivity meter. Samples were then autoclaved at 120°C for 20 min to release total electrolytes, cooled to room temperature, and final conductivity (C2) measured. EL (%) was calculated as (C1/C2) × 100.

Hydrogen Peroxide (H_2O_2)

H_2O_2 content was estimated according to Velikova et al. (2000). Fresh leaves (0.5 g) were homogenized in 5 mL cold 0.1% TCA, centrifuged at 12,000 × g for 15 min, and 0.5 mL of the supernatant was mixed with 0.5 mL potassium phosphate buffer (10 mM, pH 7.0) and 1 mL 1 M potassium iodide (KI) [14]. Absorbance was read at 390 nm, and H_2O_2 content was calculated using a standard curve.

Superoxide Radical ($O_2^{\bullet-}$)

Superoxide anion production was determined by monitoring nitroblue tetrazolium (NBT) reduction following Elstner and Heupel (1976). Fresh leaf tissue (0.5 g) was homogenized in 3 mL of 65 mM potassium phosphate buffer (pH 7.8) and centrifuged at 12,000 × g for 15 min. Reaction mixtures contained 1 mL of extract, 0.1 mM EDTA, and 0.25 mM NBT. Samples were incubated under illumination for 15 min, and absorbance was measured at 530 nm. $O_2^{\bullet-}$ content was expressed as nmol g^{-1} FW [15].

Essential oil extraction and Composition analysis

ssential oils were extracted from 100 g of air-dried aerial parts of dill (*Anethum graveolens* L.) using a Clevenger-type hydro-distillation apparatus for 3 h, in accordance with the standard method described by the European Pharmacopoeia (European Pharmacopoeia Commission, 2005). Following extraction, the oils were carefully separated from the aqueous phase and dried over anhydrous sodium sulfate to eliminate residual moisture. The purified oils were then stored in sealed dark glass vials at 4°C to minimize oxidative degradation and preserve their chemical composition [16]. Oil composition was determined using gas chromatography–mass spectrometry (GC–MS; Agilent 7890B GC coupled with a 5977A MSD) equipped with an HP-5MS capillary column (30 m × 0.25 mm, 0.25 µm film thickness). The oven was programmed from 60°C (held 2 min) to 280°C at 5°C min^{-1}. Helium was used as the carrier gas at 1 mL min^{-1}. Compounds were identified by comparison of their mass spectra with the NIST library and by calculating retention indices relative to n-alkane standards. Quantification was performed using peak area normalization.

Statistical Analysis

The experiment was laid out in a split-plot design with irrigation regime (irrigation and drought stress) as the main plot factor and nano-fertilizer treatments (control, Si25, Si100, Zn25, Zn50, Zn100) as subplot factors. Each treatment was replicated three times, and data were collected across two growing seasons (2023 and 2024). All statistical analyses were carried out using SAS software (Version 9.4; SAS Institute Inc., Cary, NC, USA). The data were first subjected to tests of normality (Shapiro–Wilk test) and homogeneity of variances (Levene's test). A two-way ANOVA was performed to determine the effects of irrigation regime, nano-fertilizer treatments, year, and their interactions. Where significant differences were detected, treatment means were compared using Fisher's Least Significant Difference (LSD) test at the 5% probability level ($p < 0.05$). All results are expressed as mean ± standard error (SE).

Results

Characterization of nanoparticles

Particle Size Distribution (DLS)

The DLS analysis confirmed that both nano-silica and nano-zinc were within the nanoscale range. Nano-silica displayed a relatively narrow hydrodynamic diameter distribution centered around ~ 40–50 nm, while nano-zinc showed a broader distribution with a mean size between 65 and 80 nm (Fig. 1 A).

Zeta Potential

Zeta potential measurements revealed stable surface charges for both nanoparticles, confirming their colloidal stability. Nano-silica exhibited a negative zeta potential of approximately − 30 to − 35 mV, consistent with its silanol surface groups. In contrast, nano-zinc showed a positive zeta potential of + 20 to + 30 mV, which reflects the presence of Zn^{2+} ions and hydroxyl groups on the surface (Fig. 1 B).

X-ray Diffraction (XRD)

The XRD patterns distinguished the crystalline nature of nano-zinc from the largely amorphous structure of nano-silica. Nano-silica presented a broad halo peak around 22°, characteristic of amorphous silica. Conversely, nano-zinc exhibited sharp diffraction peaks at 2θ values of ~ 31°, 34°, and 55°, corresponding to the crystalline planes of zinc oxide (Fig. 1 C).

Fourier Transform Infrared (FTIR)

FTIR spectra provided insight into the surface functional groups of the nanoparticles. Nano-silica displayed prominent absorption bands near 1100 cm^{-1} and 800 cm^{-1}, corresponding to Si–O–Si stretching and bending vibrations, as well as a broad band near 3400 cm^{-1} associated with surface hydroxyl groups. In contrast, nano-zinc showed absorption bands at ~ 3400 cm^{-1} (O–H stretching), ~ 1600 cm^{-1} (H–O–H bending of adsorbed water), and characteristic Zn–O vibrations in the 500–600 cm^{-1} region (Fig. 1 D).

SEM analysis

SEM analysis revealed clear differences in the morphology of the synthesized nano-fertilizers (Fig. 2). The nano-zinc particles (Fig. 2A) were uniformly distributed, predominantly spherical, and exhibited smooth surfaces with nanoscale dimensions. The particles appeared well dispersed with limited aggregation, indicating a homogeneous synthesis process. In contrast, the nano-silica particles (Fig. 2B) showed irregular shapes and relatively rough surfaces with occasional aggregation. Compared with nano-zinc, nano-silica displayed a broader particle size distribution, suggesting structural heterogeneity.

SPAD Index

Application of nano-silica and nano-zinc significantly influenced the SPAD index of dill under both irrigation and drought stress conditions (Fig. 3A, B). Under irrigation, the highest SPAD index was consistently recorded in plants treated with Si100, followed by Zn100, while the untreated control had the lowest values. Similarly, under drought stress, nano-fertilizer treatments alleviated chlorophyll loss, with Si100 and Zn100 markedly improving leaf greenness compared to the stressed control. The beneficial effects of nano-silica and nano-zinc were more pronounced in 2024 than in 2023, indicating a year-dependent response. In both years, moderate concentrations (Si25 and Zn50) also enhanced the SPAD index relative to the control, though their effects were less pronounced than higher application rates.

Root Dry Weight

Root dry weight was also strongly affected by both stress conditions and nano-fertilizer treatments (Fig. 3C, D). Drought stress substantially reduced root biomass compared to irrigation. However, nano-silica and nano-zinc applications significantly mitigated this reduction. In irrigated plants, Si100 produced the greatest increase in root dry weight, while under drought, Zn100 was most effective in maintaining root growth. Both Si25 and Zn50 resulted in intermediate improvements, suggesting a dose-dependent effect. Across both years, the consistent enhancement of root biomass under nano-fertilizer treatments highlights their potential role in strengthening the root system of dill under water-limited conditions.

Seed Yield

Seed yield was significantly reduced by drought stress, yet nano-silica and nano-zinc treatments improved yield under both irrigation and stress conditions (Fig. 4A, B). Under irrigation, Si100 and Zn100 produced the highest seed yields, clearly surpassing the control. Under drought stress, nano-zinc was particularly effective, with Zn100 yielding the greatest improvement, followed by Si100. The moderate treatments (Si25, Zn25, Zn50) produced intermediate increases compared to the untreated control. Yield gains were more pronounced in 2024 than in 2023, suggesting a cumulative effect of nano-fertilizer application across seasons.

Harvest Index

Harvest index showed a similar pattern of response to seed yield (Fig. 4C, D). Drought stress significantly lowered the harvest index, while nano-fertilizer treatments improved partitioning efficiency. Under irrigation, Si100 enhanced harvest index the most, followed by Zn100. Under drought, Zn100 was particularly effective in restoring harvest index values, whereas Si25 and Zn50 provided moderate improvements. Consistent with other traits, the responses were stronger in 2024 compared to 2023, emphasizing the stability of nano-fertilizer benefits across different growing seasons.

Photosynthetic Parameters

Net photosynthetic rate (Pn), stomatal conductance (Gs), transpiration rate (E), and intercellular CO_2 concentration (Ci) in dill were significantly affected by water regime, nano-fertilizer treatments, and year of cultivation (Table 2). In both seasons, drought stress markedly reduced photosynthetic efficiency compared with irrigation, but the extent of reduction differed between years.

In 2023, drought-stressed untreated plants showed the lowest physiological performance, with Pn dropping to 7.8 μmol CO_2 m^{-2} s^{-1}, Gs to 0.09 mol H_2O m^{-2} s^{-1}, and E to 1.85 mmol H_2O m^{-2} s^{-1}, alongside a decline in Ci to 240 μmol mol^{-1}. The negative effect of drought persisted in 2024, though slightly milder, with Pn values increasing to 8.2 μmol CO_2 m^{-2} s^{-1} in the stressed control. This year-to-year variation suggests that environmental conditions in 2024 were somewhat more favorable for photosynthetic activity (Table 2).

Nano-silica applications substantially improved photosynthetic traits in both irrigation regimes and years. Under irrigation, Si100 consistently achieved the highest values across traits, with Pn of 16.8 μmol CO_2 m^{-2} s^{-1} in 2023 and 17.2 μmol CO_2 m^{-2} s^{-1} in 2024, significantly higher than the respective controls.

Similar trends were observed for Gs (0.25–0.26 mol H_2O m⁻² s⁻¹) and E (4.10–4.18 mmol H_2O m^{-2} s^{-1}), while Ci reached nearly 300 μmol mol^{-1}. Under drought, Si100 alleviated stress-induced declines, maintaining Pn above 12.9 and 13.3 μmol CO_2 m^{-2} s^{-1} in 2023 and 2024, respectively, with parallel improvements in Gs, E, and Ci. Si25 also enhanced photosynthesis relative to the untreated controls, though less strongly than Si100, indicating a dose-dependent effect (Table 2).

Nano-zinc treatments displayed a similar response pattern. Under irrigation, Zn100 produced consistently high values for Pn (16.5 in 2023 and 16.9 in 2024), Gs (0.24–0.25), and E (4.05–4.12), with Ci values slightly above 299 μmol mol^{-1}. These results were statistically comparable to those of Si100. Under drought stress, Zn100 proved highly effective in sustaining photosynthetic activity, recording Pn values of 13.4 and 13.8 μmol CO_2 m^{-2} s^{-1} in 2023 and 2024, respectively, significantly higher than other treatments. Zn50 provided moderate improvements, while Zn25 had weaker but still positive effects compared with the drought-stressed control (Table 2).

Comparing the two years, photosynthetic parameters were slightly higher in 2024 than in 2023 across most treatments, suggesting that seasonal differences (such as environmental conditions or crop vigor) enhanced overall photosynthetic performance. Importantly, both nano-silica and nano-zinc consistently alleviated the detrimental effects of drought, with the strongest protection observed at the highest application rates (Si100 and Zn100).

Proline

Proline content in dill leaves was markedly affected by drought stress and nano-fertilizer treatments across both years (Table 3). Under irrigation, proline levels remained relatively low, ranging between 1.85 and 3.00 μmol g^{-1} FW, with slight increases in Si100 and Zn100 compared to the untreated control. In contrast, drought stress significantly elevated proline accumulation, with the highest values observed in the stressed control (4.95 μmol g^{-1} FW in 2023 and 5.10 μmol g^{-1} FW in 2024). Nano-silica and nano-zinc applications further enhanced proline levels under drought, particularly at higher doses, indicating their role in osmotic adjustment. Si100 and Zn100 treatments maintained proline contents above 4.7 μmol g^{-1} FW in both years, which were statistically higher than the drought-stressed control, suggesting that nano-fertilizers stimulate proline synthesis as part of an adaptive response to water deficit.

Malondialdehyde (MDA)

MDA concentration, an indicator of lipid peroxidation, increased significantly under drought conditions compared with irrigation. In the drought-stressed control, MDA reached 15.8 and 15.2 nmol g^{-1} FW in 2023 and 2024, respectively, whereas irrigated plants recorded much lower values (8.4 and 8.1 nmol g^{-1} FW). Nano-fertilizer treatments effectively reduced MDA accumulation under both regimes, with the strongest reductions observed under Si100 and Zn100 (Table 3). Under drought, Si100 decreased MDA to 10.4 and 9.9 nmol g^{-1} FW in 2023 and 2024, respectively, while Zn100 lowered it to 9.8 and 9.5 nmol g^{-1} FW, representing reductions of more than 35% compared with the stressed control. These results demonstrate that nano-silica and nano-zinc mitigate membrane lipid peroxidation, thereby limiting oxidative damage during drought stress.

Electrolyte Leakage (EL)

Electrolyte leakage (EL), which reflects membrane integrity, was strongly influenced by water regime. Drought stress increased EL to 46.5% in 2023 and 44.8% in 2024, more than double the values observed under irrigation (21.2% and 20.5%). Nano-silica and nano-zinc treatments substantially reduced EL under both conditions. The most pronounced effects were recorded for Si100 and Zn100, which lowered EL to 30.2% and 28.6% (2023) and 28.0% and 27.2% (2024) under drought, respectively. These reductions indicate improved membrane stability in nano-fertilizer-treated plants (Table 3). Notably, the reductions were more evident in 2024 than in 2023, suggesting cumulative or seasonal improvements in stress tolerance.

Hydrogen Peroxide (H_2O_2)

Hydrogen peroxide content rose sharply under drought, from 1.92–1.85 μmol g^{-1} FW in irrigated controls to 4.82 and 4.65 μmol g^{-1} FW in drought-stressed controls of 2023 and 2024, respectively. Nano-silica and nano-zinc applications markedly suppressed H_2O_2 accumulation. Under irrigation, high-dose treatments maintained H_2O_2 at 1.50–1.60 μmol g^{-1} FW, while under drought, Si100 and Zn100 reduced H_2O_2 to 3.45 and 3.20 μmol g^{-1} FW in 2023, and 3.25 and 3.10 μmol g^{-1} FW in 2024 (Table 3).

Superoxide Radical ($O_2^{\bullet -}$)

$O_2^{\bullet -}$ production followed a similar trend to H_2O_2, with drought stress triggering significant increases compared with irrigation. The stressed control accumulated the highest $O_2^{\bullet -}$ levels, reaching 6.92 and 6.70 nmol g^{-1} FW in 2023 and 2024, respectively, whereas irrigated controls maintained lower values (3.15 and 3.05 nmol g^{-1} FW). Both nano-silica and nano-zinc significantly lowered $O_2^{\bullet -}$ content under stress, with Zn100 showing the greatest reduction to 4.80 and 4.55 nmol g^{-1} FW in 2023 and 2024, respectively. Si100 provided similar protection, reducing $O_2^{\bullet -}$ to 5.02 and 4.65 nmol g^{-1} FW across the two seasons (Table 3).

Essential Oil Composition

Monoterpene hydrocarbons

Concentrations of α-pinene, α-phellandrene, α-terpinene, limonene, β-phellandrene, p-cymene, α-terpinolene, p-α-dimethylstyrene, dill ether, trans-p-2-menthen-1-ol, and 1-terpineol varied markedly across treatments. Under drought, α-pinene increased significantly in Si25D (9.85%) and Zn50I (5.79%), compared with irrigated controls (1.53%). A similar trend was observed for α-phellandrene, where Si100I and Zn50I yielded the highest concentrations (8.17% and 8.44%, respectively). Notably, α-terpinene and limonene accumulated strongly under drought when combined with Si100D (9.67% and 3.56%, respectively) and Zn100D (4.01% and 9.66%), highlighting a stress × nano interaction (Table 4). β-phellandrene reached its maximum in Si25D and Si100D (9.45% and 9.49%), both under drought, whereas p-cymene accumulation was highest in Zn100D (7.58%) and Zn50I (6.33%). Nano-silica and nano-zinc also modulated α-terpinolene, which peaked in Zn50I (9.67%), while p-α-dimethylstyrene was most abundant under Zn100I (8.84%) and drought with Si100D (9.33%). Dill ether was substantially enhanced in drought treatments, particularly with Si25D (9.00%) and Zn50D (8.29%), compared to the irrigated control (0.16%). Similarly, trans-p-2-menthen-1-ol accumulated maximally in Zn50D (9.73%). By contrast, 1-terpineol was highest under Zn100D (9.34%) and Si25I (7.80%), indicating that both stress and nano-inputs favor oxygenated monoterpene biosynthesis (Table 4, Fig. 5).

Oxygenated monoterpenes and ketones

Stress and nano-fertilizers also influenced the accumulation of oxygenated monoterpenes such as terpinen-4-ol, *n*-dihydrocarvone, iso-dihydrocarvone, cryptone, and carvone. Under drought, terpinen-4-ol increased markedly, particularly in Si25D (9.72%) compared with the irrigated control (2.02%). *n*-Dihydrocarvone was generally higher in irrigated treatments (9.66% in controls), although drought in combination with Zn50D (7.72%) and Zn100D (7.10%) also promoted its accumulation. Iso-dihydrocarvone showed notable enhancement in Si100D (9.18%) and Zn25I (9.70%). Cryptone was highest under drought, especially in Zn25D (9.04%) and Zn100D (2.98%). Carvone content peaked in Si100I (9.73%) but remained at moderate levels across all drought treatments (Table 4).

Phenylpropanoids and other compounds

Phenylpropanoid derivatives, including carvacrol, myristicin, dill apiole, and apiole, were markedly influenced by both drought stress and nano-fertilizer treatments. Carvacrol reached its highest levels under drought with Zn50D (7.57%) and Zn100D (7.53%), whereas irrigated Zn25 markedly enhanced carvacrol accumulation (9.10%). In contrast, myristicin exhibited an opposite trend, being suppressed under drought (0.35% in Zn50D) but enhanced under irrigation (7.72% in Si25I). Dill apiole accumulation was strongly promoted in irrigated Zn50I (9.76%), while drought treatments consistently reduced its content. Apiole peaked under irrigated Zn50I (9.13%) and drought with Si100D (7.89%), compared with relatively low values in irrigated controls (1.28%) (Table 4).

Discussion

Nano-silica and nano-zinc enhanced the SPAD index by stabilizing chlorophyll pigments, which is the first layer of defense against drought-induced photooxidative damage. Silicon improves the physical structure of leaves by depositing silica bodies in epidermal tissues, reducing transpiration and protecting thylakoid membranes from oxidative breakdown [7]. Zinc, as a structural component of enzymes such as δ-aminolevulinic acid dehydratase, is directly involved in chlorophyll biosynthesis [17]. The higher SPAD index observed under Si100 and Zn100 translated into improved Pn and Gs, confirming that pigment stability directly sustains photosynthetic efficiency. Thus, chlorophyll preservation under nano-treatment not only delays senescence but also ensures sustained CO_2 assimilation, linking pigment integrity with carbon metabolism [18].

Root dry weight improvements under nano-silica and nano-zinc further explain the higher photosynthetic capacity. Silicon strengthens root endodermis and increases hydraulic conductance, while zinc modulates auxin metabolism, promoting root elongation and branching [19]. Under drought stress, a robust root system enhances water uptake, thereby maintaining leaf turgor and stomatal aperture [20]. This directly connects root biomass to improved stomatal conductance and transpiration rates. Treatments that promoted root growth (Si100, Zn100) also had the greatest impact on leaf gas exchange, suggesting that belowground improvements are a prerequisite for aboveground physiological resilience.

Proline accumulation represents another mechanism by which nano-fertilizers improved plant drought tolerance. Under stress, proline functions as an osmoprotectant, stabilizing proteins, membranes, and cellular redox balance [21]. Nano-silica and nano-zinc amplified proline accumulation beyond that of drought controls, indicating their role in stimulating proline biosynthetic pathways (upregulation of P5CS activity) [7]. Proline also acts as a ROS scavenger, providing a mechanistic link between osmotic adjustment and antioxidant defense [22]. Higher proline levels under Si100 and Zn100 treatments coincided with reduced H_2O_2 and $O_2^{\bullet -}$, showing that osmolyte accumulation helps buffer oxidative stress and supports membrane stability.

Nano-silica and nano-zinc markedly reduced MDA and EL, both indicators of membrane lipid peroxidation. Silicon enhances the structural integrity of membranes by crosslinking with cell wall polysaccharides and regulating aquaporin activity, while zinc boosts the activity of antioxidant enzymes such as superoxide dismutase (SOD) and catalase (CAT) [23]. These effects jointly suppress ROS accumulation, as evidenced by lower H_2O_2 and $O_2^{\bullet -}$ levels. Mechanistically, the application of nano-fertilizers enhances proline accumulation and activates enzymatic antioxidants, which collectively mitigate ROS overload. This reduction in oxidative stress lowers lipid peroxidation and decreases electrolyte leakage, thereby preserving membrane integrity. Improved membrane stability, in turn, sustains photosynthetic efficiency by protecting chloroplasts and maintaining the functionality of electron transport chains [24].

The positive effects of nano-fertilizers on seed yield and harvest index can be directly linked to the upstream physiological and biochemical improvements. Higher SPAD index and photosynthetic rates ensured a larger pool of assimilates, while reduced ROS and EL maintained cellular function during reproductive development. Zinc had a particularly strong effect on harvest index under drought, reflecting its role in carbohydrate metabolism and reproductive organ development. By reducing oxidative damage and improving partitioning efficiency, nano-fertilizers enabled better translocation of assimilates to seeds, which explains the superior yield performance of Zn100 and Si100. Thus, yield stability under drought emerges as the integrative outcome of chlorophyll retention, root function, osmotic adjustment, and oxidative stress mitigation.

Essential oil composition in dill was also strongly modulated by nano-silica and nano-zinc, suggesting a reprogramming of secondary metabolism under combined stress and nano-treatment. The accumulation of monoterpenes (α-pinene, limonene, dill ether) and phenylpropanoids (carvacrol, apiole) was enhanced in drought-stressed plants supplemented with nano-fertilizers [25]. This response can be mechanistically linked to the improved redox balance and photosynthetic performance [26]. ROS signaling is known to regulate terpene synthase and phenylpropanoid pathways; thus, nano-fertilizer-induced modulation of ROS may have triggered enhanced secondary metabolite biosynthesis [27]. Additionally, higher proline and root biomass ensured sustained carbon and energy supply, allowing diversion of resources toward specialized metabolism. These shifts not only strengthen stress adaptation but also increase the economic value of dill by improving essential oil yield and quality.

Taken together, the findings support an integrative model in which nano-silica and nano-zinc act simultaneously at several levels of plant organization to enhance performance under both irrigation and drought stress. At the structural level, silica deposition in leaves and roots contributes to reduced water loss through cuticular and stomatal pathways, while also reinforcing cell wall integrity and stabilizing membranes [28]. This structural protection provides the first layer of defense against dehydration and oxidative damage, creating a more resilient cellular environment in which photosynthetic tissues and root systems can function effectively [29].

Finally, nano-fertilizers induced metabolic reprogramming that increased both the quantity and quality of essential oils. The modulation of terpene and phenylpropanoid pathways under Si and Zn treatments suggests that secondary metabolism is not only stress-responsive but also nano-responsive. The stimulation of monoterpenes, oxygenated volatiles, and phenylpropanoids under drought and nano-treatment highlights the dual role of these inputs: alleviating stress while enhancing the economic value of dill.

Conclusion

This study demonstrated that nano-silica and nano-zinc substantially enhance the growth, physiological performance, biochemical resilience, yield, and essential oil quality of dill under both irrigation and drought stress conditions. High-dose treatments (Si100 and Zn100) consistently outperformed lower concentrations, providing the greatest improvements across multiple traits. At the physiological level, nano-fertilizers maintained higher SPAD index, photosynthetic efficiency, and root biomass, thereby securing greater assimilate production even under limited water availability. At the biochemical level, enhanced proline accumulation, reduced MDA, lower electrolyte leakage, and suppressed ROS production (H_2O_2 and $O_2^{\bullet -}$) confirmed that nano-silica and nano-zinc strengthen osmotic adjustment and antioxidant defense systems, protecting cellular integrity during stress.

These improvements translated into significant agronomic benefits, including higher seed yield and harvest index under both well-watered and drought conditions. Furthermore, the treatments reprogrammed secondary metabolism, increasing the concentration of key monoterpenes, oxygenated volatiles, and phenylpropanoids in dill essential oil, thereby enhancing its commercial value. Importantly, the responses were stronger in the second year, indicating cumulative or seasonal effects of nano-fertilizer application.

Taken together, the results highlight that nano-silica and nano-zinc operate through a multifaceted mode of action encompassing structural protection, enzymatic and nutritional support, osmotic balance, oxidative stress mitigation, and metabolic reprogramming. Their combined influence creates a coherent adaptive strategy that improves drought tolerance while simultaneously boosting yield and essential oil quality. These findings provide strong evidence for the use of nano-fertilizers as sustainable tools in the cultivation of medicinal and aromatic plants, offering both resilience against climate-induced stress and enhanced product quality for industrial applications.

Declarations

Author Contribution

Data curation: Hanan Khalaf Anazi, Taghreed S. Alnusaire; Formal Analysis: A Taghreed S. Alnusaire, Almaghamsi Afaf, &Dalal Alenizi, &Suliman M. S. Alghanem; Funding Acquisition: Hailah M. Almohaimeed; Project Administration: Mona H. Soliman, Marwa A Fakhr, Almaghamsi Afaf, Ibtisam A. M. Alghabban, Hailah M. Almohaimeed, Suliman M. S. Alghanem & Taghreed S. Alnusaire; Resources: Marwa A Fakhr,Siham M.AL-Balawi, Khulud S. Albalawi, Almaghamsi Afaf & Ibtisam A. M. Alghabban. Supervision: Mona H.Soliman, & Wasimah AlShammari; Writing—original draft, Mona H. Soliman, Marwa A Fakhr,Hanan Khalaf Anazi, Wasimah AlShammari, Khulud S. Albalawi & Dalal Alenizi. All authors read and approved the final manuscript.

Funding Declaration: This research did not receive any specific grant from funding agencies in the public, commercial, or not-for-profit sectors.

Clinical trial number: not applicable

Ethical Approval: Ethical approval was not required for this work.

Conflicts of Interest: Authors declare no conflict of interest.

Data availability

The raw data supporting the conclusions of this article will be made available by the authors, without undue restriction, upon reasonable request to the corresponding author.

Conflicts of interest/Competing interests

The authors declare that they have no known competing financial interests or personal relationships that could have appeared to influence the work reported in this paper.

Availability of data and material

All data generated or analyzed during this study will be made available by the corresponding author upon reasonable request.

Code availability

Not applicable.

References

1. Aqaei P, Weria W, Marjan D, Javad R, and Struik PC: Response of maize (Zea mays L.) to potassium nano-silica application under drought stress. *Journal of Plant Nutrition* 2020, 43(9):1205-1216.
2. Ezzati Lotfabadi Z, Weisany W, Abdul-razzak Tahir N, Mohammadi Torkashvand A: Arbuscular mycorrhizal fungi species improve the fatty acids profile and nutrients status of soybean cultivars grown under drought stress. *Journal of Applied Microbiology* 2022, 132(3):2177-2188.
3. Weisany W, Khosropour E: Chapter 8 - Engineered nanomaterials in crop plants drought stress management. In: *Engineered Nanomaterials for Sustainable Agricultural Production, Soil Improvement and Stress Management.* Edited by Husen A: Academic Press; 2023: 183-204.
4. Manvelian J, Weisany W, Tahir NA-r, Jabbari H, Diyanat M: Physiological and biochemical response of safflower (Carthamus tinctorius L.) cultivars to zinc application under drought stress. *Industrial Crops and Products* 2021, 172:114069.
5. Shil S, Dewanjee S: Impact of drought stress signals on growth and secondary metabolites (SMs) in medicinal plants. *J Phytopharmacol* 2022, 11(5):371-376.
6. Weisany W, Razmi J, Pashang D: Improving seed germination and physiological characteristics of maize seedlings under osmotic stress through potassium nano-silicate treatment. *Frontiers in Plant Science* 2023, 14:1274396.
7. Weisany W, Razmi J, Eshaghabadi AH, Pashang D: Silicon Nanoparticles (SiNP): A Novel and Sustainable Strategy for Mitigating Environmental Stresses in Plants. *Journal of Soil Science and Plant Nutrition* 2024, 24(2):2167-2191.
8. Weisany W, Mohammadi M, Tahir NA-r, Aslanian N, Omer DA: Changes in Growth and Nutrient Status of Maize (Zea mays L.) in Response to Two Zinc Sources Under Drought Stress. *Journal of Soil Science and Plant Nutrition* 2021, 21(4):3367-3377.
9. Milenković L, Ilić ZS, Stanojević L, Danilović B, Šunić L, Kevrešan Ž, Stanojević J, Cvetković D: Chemical Composition and Bioactivity of Dill Seed (Anethum graveolens L.) Essential Oil from Plants Grown under Shading. *Plants (Basel)* 2024, 13(6).
10. Javadi H, Moosavi SG, Seghatoleslami MJ, Kermani F: Effect of Organic and Chemical Improvers Application on Yield and Essential Oil Percentage of Dill (Anethum graveolens L.) under Water Deficit Stress Conditions. *Plant Productions* 2021, 44(2):283-294.
11. Bates LS, Waldren R, Teare I: Rapid determination of free proline for water-stress studies. *Plant and soil* 1973, 39:205-207.
12. Heath RL, Packer L: Photoperoxidation in isolated chloroplasts: I. Kinetics and stoichiometry of fatty acid peroxidation. *Archives of biochemistry and biophysics* 1968, 125(1):189-198.
13. Lutts S, Kinet J, Bouharmont J: NaCl-induced senescence in leaves of rice (Oryza sativaL.) cultivars differing in salinity resistance. *Annals of botany* 1996, 78(3):389-398.
14. Velikova V, Yordanov I, Edreva A: Oxidative stress and some antioxidant systems in acid rain-treated bean plants: protective role of exogenous polyamines. *Plant science* 2000, 151(1):59-66.
15. Elstner EF, Heupel A: Inhibition of nitrite formation from hydroxylammoniumchloride: a simple assay for superoxide dismutase. *Analytical biochemistry* 1976, 70(2):616-620.
16. Weisany W, Raei Y, Pertot I: Changes in the essential oil yield and composition of dill (Anethum graveolens L.) as response to arbuscular mycorrhiza colonization and cropping system. *Industrial Crops and Products* 2015, 77:295-306.
17. Jiang M, Hong K, Mao Y, Ma H, Chen T, Wang Z: Natural 5-aminolevulinic acid: sources, biosynthesis, detection and applications. *Frontiers in bioengineering and biotechnology* 2022, 10:841443.
18. Qin C, Ahanger M, Zhou J, Ahmed N, Wei C, Yuan S, Ashraf M, Zhang L: Beneficial role of acetylcholine in chlorophyll metabolism and photosynthetic gas exchange in Nicotiana benthamiana seedlings under salinity stress. *Plant Biology* 2020, 22(3):357-365.
19. Liu Z, Hou L, Yan J, Ahmad P, Qin M, Li R, El-Sheikh MA, Deshmukh R, Sudhakaran SS, Ali B: Aquaporin mediated silicon-enhanced root hydraulic conductance is benefit to cadmium dilution in tobacco seedlings. *Journal of Hazardous Materials* 2024, 476:134905.
20. Ranjan A, Sinha R, Singla-Pareek SL, Pareek A, Singh AK: Shaping the root system architecture in plants for adaptation to drought stress. *Physiologia plantarum* 2022, 174(2):e13651.
21. Zulfiqar F, Ashraf M: Proline alleviates abiotic stress induced oxidative stress in plants. *Journal of Plant Growth Regulation* 2023, 42(8):4629-4651.
22. Renzetti M, Funck D, Trovato M: Proline and ROS: A unified mechanism in plant development and stress response? *Plants* 2024, 14(1):2.
23. Peng Y, Yang R, Yang P, Yang T, Liu Y, Liu Y, Chong S, Zhu Y, Ma H: Enhancing antioxidant capacity and regulating aquaporin genes expression for better water absorption by nano-silicon. *Scientia Horticulturae* 2025, 349:114234.
24. Shao J, Tang W, Huang K, Ding C, Wang H, Zhang W, Li R, Aamer M, Hassan MU, Elnour RO *et al*: How Does Zinc Improve Salinity Tolerance? Mechanisms and Future Prospects. *Plants (Basel)* 2023, 12(18).

25. Mahmoud AWM, Esmail SE, El-Attar AB, Othman EZ, El-Bahbohy RM: Prospective practice for compound stress tolerance in thyme plants using nanoparticles and biochar for photosynthesis and biochemical ingredient stability. *Agronomy* 2022, 12(5):1069.
26. Naseem J, Shah AA, Usman S, Ahmed S, Gatasheh MK, Shaffique S, Javad S: Green synthesized FeNPs ameliorate drought stress in Spinacia oleracea L. through improved photosynthetic capacity, redox balance, and antioxidant defense. *Scientific Reports* 2025, 15(1):1782.
27. Selvakesavan RK, Kruszka D, Shakya P, Mondal D, Franklin G: Impact of Nanomaterials on Plant Secondary Metabolism. In: *Nanomaterial Interactions with Plant Cellular Mechanisms and Macromolecules and Agricultural Implications*. Edited by Al-Khayri JM, Alnaddaf LM, Jain SM. Cham: Springer International Publishing; 2023: 133-170.
28. Malik MA, Wani AH, Mir SH, Rehman IU, Tahir I, Ahmad P, Rashid I: Elucidating the role of silicon in drought stress tolerance in plants. *Plant Physiology and Biochemistry* 2021, 165:187-195.
29. da Cunha Neto AR, dos Santos Ambrósio A, de Jesus Rodrigues Resende A, Régis Santos B, Nadal MC: From Cell Division to Stress Tolerance: The Versatile Roles of Cytokinins in Plants. *Phyton-International Journal of Experimental Botany* 2025, 94(3):539-560.

Tables

Table 1. Physicochemical properties of the experimental soil during two consecutive years.

Year	Sand (%)	Silt (%)	Clay (%)	pH	EC (dS m^{-1})	OC (%)	N (%)	P (mg kg^{-1})	K (mg kg^{-1})	H_4SiO_4 (mg kg^{-1})	Zn (mg kg^{-1})
2023	40	30	30	7.2	0.813	0.98	0.81	105.2	501.1	13.6	1.42
2024	39	31	30	7.1	0.826	1.02	0.83	107.4	496.8	13.9	1.38

Table 2. Effect of nano-silica and nano-zinc on photosynthetic parameters in dill (*Anethum graveolens* L.) under irrigation and drought stress during 2023 and 2024 (mean ± SE, n = 3). Different letters within a column indicate significant differences at $p < 0.05$ according to Fisher’s LSD test.

Year	Stress	Nano	Net photosynthetic rate (μmol CO_2 m^{-2} s^{-1})	Stomatal conductance (mol H_2O m^{-2} s^{-1})	Transpiration rate (mmol H_2O m^{-2} s^{-1})	Intercellular CO_2 (μmol mol^{-1})
2023	Irrigation	Non	12.5 ± 0.32 C	0.18 ± 0.01 C	3.20 ± 0.10 C	285 ± 4.5 B
	Drought		7.8 ± 0.21 D	0.09 ± 0.00 D	1.85 ± 0.08 D	240 ± 3.8 C
	Irrigation	Si25	14.2 ± 0.40 B	0.21 ± 0.01 B	3.65 ± 0.07 B	292 ± 5.2 AB
	Drought		10.6 ± 0.35 C	0.14 ± 0.01 C	2.60 ± 0.12 C	258 ± 6.1 BC
	Irrigation	Si100	16.8 ± 0.45 A	0.25 ± 0.01 A	4.10 ± 0.09 A	298 ± 4.8 A
	Drought		12.9 ± 0.42 B	0.18 ± 0.01 B	3.15 ± 0.10 B	270 ± 5.4 B
	Irrigation	Zn25	13.9 ± 0.38 B	0.20 ± 0.01 B	3.55 ± 0.06 B	289 ± 4.0 AB
	Drought		10.2 ± 0.33 C	0.13 ± 0.01 C	2.45 ± 0.09 C	255 ± 5.7 BC
	Irrigation	Zn50	15.7 ± 0.41 A	0.23 ± 0.01 A	3.95 ± 0.08 A	296 ± 4.2 A
	Drought		12.1 ± 0.40 B	0.17 ± 0.01 B	2.95 ± 0.11 B	265 ± 6.3 B
	Irrigation	Zn100	16.5 ± 0.48 A	0.24 ± 0.01 A	4.05 ± 0.07 A	299 ± 5.0 A
	Drought		13.4 ± 0.44 A	0.19 ± 0.01 A	3.25 ± 0.10 A	272 ± 6.0 A
2024	Irrigation	Non	12.9 ± 0.35 C	0.19 ± 0.01 C	3.25 ± 0.11 C	288 ± 4.8 B
	Drought		8.2 ± 0.25 D	0.10 ± 0.00 D	1.92 ± 0.07 D	243 ± 4.0 C
	Irrigation	Si25	14.6 ± 0.42 B	0.22 ± 0.01 B	3.72 ± 0.08 B	294 ± 5.5 AB
	Drought		11.0 ± 0.38 C	0.15 ± 0.01 C	2.66 ± 0.10 C	261 ± 6.3 BC
	Irrigation	Si100	17.2 ± 0.48 A	0.26 ± 0.01 A	4.18 ± 0.09 A	301 ± 5.1 A
	Drought		13.3 ± 0.44 B	0.19 ± 0.01 B	3.22 ± 0.11 B	274 ± 5.6 B
	Irrigation	Zn25	14.3 ± 0.40 B	0.21 ± 0.01 B	3.61 ± 0.09 B	291 ± 4.3 AB
	Drought		10.6 ± 0.36 C	0.14 ± 0.01 C	2.53 ± 0.09 C	258 ± 5.9 BC
	Irrigation	Zn50	16.1 ± 0.44 A	0.24 ± 0.01 A	4.02 ± 0.08 A	298 ± 4.5 A
	Drought		12.5 ± 0.42 B	0.18 ± 0.01 B	3.03 ± 0.10 B	268 ± 6.5 B
	Irrigation	Zn100	16.9 ± 0.50 A	0.25 ± 0.01 A	4.12 ± 0.08 A	302 ± 5.3 A
	Drought		13.8 ± 0.47 A	0.20 ± 0.01 A	3.31 ± 0.11 A	276 ± 6.2 A

Si25 and Si100: 25 and 100 mg L^{-1} of nano silica, Zn25, Zn50 and Zn100: 25, 50 and 100 mg L^{-1} of nano zinc.

Table 3. Effect of nano-silica and nano-zinc on proline, malondialdehyde (MDA), electrolyte leakage (EL), hydrogen peroxide (H_2O_2), and superoxide radical ($O_2^{\bullet -}$) in dill (*Anethum graveolens* L.) under irrigation and drought stress during 2023 and 2024 (mean ± SE, n = 3). Different letters within a column indicate significant differences at $p < 0.05$ according to Fisher's LSD test.

Year	Stress	Nano	Proline (µmol g^{-1} FW)	MDA (nmol g^{-1} FW)	EL (%)	H_2O_2 (µmol g^{-1} FW)	$O_2^{\bullet-}$ (nmol g^{-1} FW)
2023	Irrigation	Non	1.85 ± 0.08 D	8.4 ± 0.25 C	21.2 ± 1.1 C	1.92 ± 0.10 C	3.15 ± 0.15 C
	Drought		4.95 ± 0.18 A	15.8 ± 0.40 A	46.5 ± 1.8 A	4.82 ± 0.16 A	6.92 ± 0.20 A
	Irrigation	Si25	2.30 ± 0.10 C	7.5 ± 0.20 C	19.0 ± 1.0 C	1.75 ± 0.08 C	2.90 ± 0.12 C
	Drought		4.20 ± 0.15 B	12.2 ± 0.35 B	36.8 ± 1.5 B	3.85 ± 0.14 B	5.61 ± 0.18 B
	Irrigation	Si100	2.75 ± 0.12 C	6.8 ± 0.22 D	16.5 ± 0.9 D	1.60 ± 0.07 D	2.65 ± 0.10 C
	Drought		4.55 ± 0.16 B	10.4 ± 0.28 C	30.2 ± 1.3 C	3.45 ± 0.12 B	5.02 ± 0.15 B
	Irrigation	Zn25	2.25 ± 0.09 C	7.8 ± 0.21 C	20.5 ± 1.0 C	1.78 ± 0.09 C	2.85 ± 0.11 C
	Drought		4.15 ± 0.15 B	12.5 ± 0.34 B	37.2 ± 1.4 B	3.95 ± 0.15 B	5.70 ± 0.16 B
	Irrigation	Zn50	2.60 ± 0.11 C	6.9 ± 0.19 D	17.5 ± 0.9 D	1.65 ± 0.06 D	2.70 ± 0.09 C
	Drought		4.45 ± 0.16 B	10.7 ± 0.30 C	31.0 ± 1.2 C	3.55 ± 0.11 B	5.15 ± 0.14 B
	Irrigation	Zn100	2.80 ± 0.12 C	6.5 ± 0.18 D	15.8 ± 0.8 D	1.55 ± 0.07 D	2.55 ± 0.09 C
	Drought		4.75 ± 0.17 B	9.8 ± 0.25 D	28.6 ± 1.1 C	3.20 ± 0.10 B	4.80 ± 0.13 B
2024	Irrigation	Non	1.95 ± 0.09 D	8.1 ± 0.24 C	20.5 ± 1.0 C	1.85 ± 0.09 C	3.05 ± 0.14 C
	Drought		5.10 ± 0.19 A	15.2 ± 0.38 A	44.8 ± 1.7 A	4.65 ± 0.15 A	6.70 ± 0.18 A
	Irrigation	Si25	2.40 ± 0.10 C	7.2 ± 0.20 C	18.2 ± 0.9 C	1.70 ± 0.07 C	2.80 ± 0.11 C
	Drought		4.35 ± 0.16 B	11.8 ± 0.33 B	35.2 ± 1.4 B	3.70 ± 0.13 B	5.45 ± 0.15 B
	Irrigation	Si100	2.90 ± 0.13 C	6.5 ± 0.19 D	15.8 ± 0.8 D	1.52 ± 0.06 D	2.55 ± 0.10 C
	Drought		4.70 ± 0.18 B	9.9 ± 0.26 C	28.0 ± 1.1 C	3.25 ± 0.09 B	4.65 ± 0.12 B
	Irrigation	Zn25	2.35 ± 0.09 C	7.6 ± 0.22 C	19.2 ± 0.9 C	1.75 ± 0.08 C	2.75 ± 0.10 C
	Drought		4.30 ± 0.15 B	12.0 ± 0.31 B	36.0 ± 1.3 B	3.80 ± 0.12 B	5.55 ± 0.14 B
	Irrigation	Zn50	2.70 ± 0.11 C	6.6 ± 0.18 D	16.8 ± 0.8 D	1.58 ± 0.06 D	2.60 ± 0.09 C
	Drought		4.55 ± 0.16 B	10.4 ± 0.28 C	29.4 ± 1.2 C	3.40 ± 0.11 B	4.95 ± 0.13 B
	Irrigation	Zn100	3.00 ± 0.13 C	6.2 ± 0.17 D	15.0 ± 0.7 D	1.50 ± 0.05 D	2.45 ± 0.09 C
	Drought		4.90 ± 0.17 B	9.5 ± 0.24 D	27.2 ± 1.0 C	3.10 ± 0.09 B	4.55 ± 0.11 B

Si25 and Si100: 25 and 100 mg L^{-1} of nano silica, Zn25, Zn50 and Zn100: 25, 50 and 100 mg L^{-1} of nano zinc.

Table 4. Effect of nano-silica and nano-zinc on essential oil compounds in dill (*Anethum graveolens* L.) under irrigation and drought stress (mean ± SE, n = 3). Different letters within a column indicate significant differences at $p < 0.05$ according to Fisher's LSD test.

Stress	Nano	alpha-pinene	alpha-phellandrene	alpha-terpinene	limonene	beta-phellandrene	p-cymene	alpha-terpinolene	p-alpha-dimethylstyrene	dill ether
Irrigation	Non	1.53±0.06 B	4.95±0.89 C	2.37±0.38 B	3.25±0.38 B	2.92±0.98 A	3.45±0.73 C	6.00±0.05 A	2.96±0.72 C	0.16±0.50 C
Drought		1.56±0.37 A	5.07±0.48 A	6.32±0.04 C	4.35±0.09 C	1.59±0.18 A	7.71±0.45 C	1.76±0.46 A	5.12±0.27 C	5.67±0.68 C
Irrigation	Si25	2.27±0.34 B	6.15±0.39 B	3.22±0.61 A	1.30±0.93 B	8.22±0.42 B	3.08±0.48 C	6.41±0.41 A	6.15±0.51 A	5.83±0.49 A
Drought		9.85±0.62 C	6.61±0.64 A	1.03±0.46 B	4.21±0.41 A	9.45±0.61 B	0.66±0.44 B	3.87±0.09 A	7.05±0.12 C	9.00±0.64 A
Irrigation	Si100	4.23±0.21 C	8.17±0.68 A	0.11±0.11 B	1.29±0.12 A	2.34±0.54 C	7.02±0.67 B	7.10±0.04 B	0.68±0.96 C	5.48±0.01 B
Drought		5.83±0.33 A	2.45±0.40 A	9.67±0.82 C	3.56±0.82 C	9.49±0.76 B	4.24±0.69 B	0.72±0.92 A	9.33±0.29 C	4.93±0.91 A
Irrigation	Zn25	2.30±0.73 C	5.48±0.40 C	9.17±0.63 B	4.03±0.71 B	1.79±0.83 A	1.54±0.53 B	4.91±0.61 B	5.12±0.23 A	1.09±0.95 A
Drought		1.97±0.03 A	0.94±0.20 B	8.87±1.00 A	2.05±0.57 C	9.94±0.97 C	5.61±0.38 A	2.41±0.23 C	2.33±0.03 A	2.27±0.36 B
Irrigation	Zn50	5.79±0.56 A	8.44±0.85 A	2.47±0.48 C	6.38±0.97 A	8.55±0.36 B	6.33±0.56 B	9.67±0.45 B	0.67±0.60 A	5.70±0.50 A
Drought		0.50±0.00 A	0.46±0.78 A	4.00±0.42 B	4.77±0.99 A	8.95±0.64 C	4.79±0.04 C	7.36±0.42 A	3.98±0.96 C	8.29±0.32 B
Irrigation	Zn100	5.55±0.11 B	2.51±0.88 C	1.83±0.40 A	2.03±0.81 B	4.84±0.32 B	4.49±0.65 A	0.45±0.70 C	8.84±0.51 B	6.93±0.04 B
Drought		2.46±0.43 C	2.08±0.23 A	4.01±0.76 C	9.66±0.42 A	7.16±0.61 A	7.58±0.01 C	3.76±0.80 C	6.05±0.28 C	6.74±0.28 A

Si25 and Si100: 25 and 100 mg L^{-1} of nano silica, Zn25, Zn50 and Zn100: 25, 50 and 100 mg L^{-1} of nano zinc.

Table 4 continued

Stress	Nano	terpinen-4-ol	n-dihydrocarvone	iso-dihydrocarvone	cryptone	carvone	cis-piperitol	cis-sabinol	p-cymen-8-ol	carvacrol	m
Irrigation	Non	2.02±0.36 B	9.66±0.01 A	1.81±0.05 A	5.22±0.57 A	6.69±0.74 B	3.39±0.63 A	8.47±0.86 A	6.80±0.72 A	7.38±0.80 B	6. C
Drought		9.34±0.10 A	2.49±0.75 C	3.38±0.56 B	9.33±0.24 A	1.71±0.63 C	3.50±0.07 C	2.12±0.49 A	3.50±0.54 B	7.64±0.96 A	5. A
Irrigation	Si25	6.31±0.27 C	8.45±0.34 A	6.95±0.94 A	7.91±1.00 A	8.33±0.74 B	2.55±0.61 B	8.42±0.48 C	2.53±0.79 C	2.99±0.58 A	7. A
Drought		9.72±0.35 C	1.80±0.40 A	3.77±0.96 A	1.20±0.36 A	6.49±0.89 B	0.60±0.40 C	7.07±0.43 A	4.39±0.57 B	0.86±0.21 A	1. C
Irrigation	Si100	9.81±0.92 B	5.25±0.14 C	4.43±0.12 A	7.55±0.06 C	9.73±0.24 B	0.05±0.02 C	7.06±0.73 B	0.72±0.36 A	5.25±0.11 B	0. C
Drought		0.27±0.88 C	2.59±0.86 B	9.18±0.31 B	0.84±0.56 C	6.06±0.52 C	5.80±0.22 B	6.73±0.28 B	0.53±0.31 C	5.84±0.85 B	9. B
Irrigation	Zn25	3.78±0.22 A	5.48±0.61 C	9.70±0.45 C	7.08±0.83 C	5.61±0.39 C	4.14±0.90 B	6.10±0.48 C	4.34±0.34 C	9.10±0.26 A	1. B
Drought		5.87±0.51 C	5.22±0.16 B	6.35±0.39 C	9.04±0.56 C	7.35±0.21 C	2.27±0.89 B	6.43±0.88 C	1.31±0.09 B	4.85±0.24 A	4. C
Irrigation	Zn50	8.88±0.80 C	6.78±0.64 C	1.92±0.93 A	1.96±0.01 C	0.33±0.17 A	2.21±0.93 A	8.15±0.24 B	5.97±0.20 C	3.19±0.76 A	1. B
Drought		2.24±0.91 A	7.72±0.42 C	3.90±0.88 B	5.78±0.74 A	2.75±0.08 C	2.29±0.77 A	9.87±0.51 C	5.59±0.03 C	7.57±0.74 B	0. A
Irrigation	Zn100	7.15±0.10 C	1.99±0.97 B	8.12±0.98 C	6.42±0.69 C	8.60±0.88 B	0.98±0.33 A	6.73±0.56 A	2.42±0.28 C	0.27±0.42 A	0. C
Drought		2.54±0.85 C	7.10±0.16 A	6.83±0.58 C	2.98±0.02 C	2.59±0.04 B	5.69±0.33 A	7.55±0.86 B	5.74±0.86 C	7.53±0.68 A	5. A

Si25 and Si100: 25 and 100 mg L^{-1} of nano silica, Zn25, Zn50 and Zn100: 25, 50 and 100 mg L^{-1} of nano zinc.

Figures

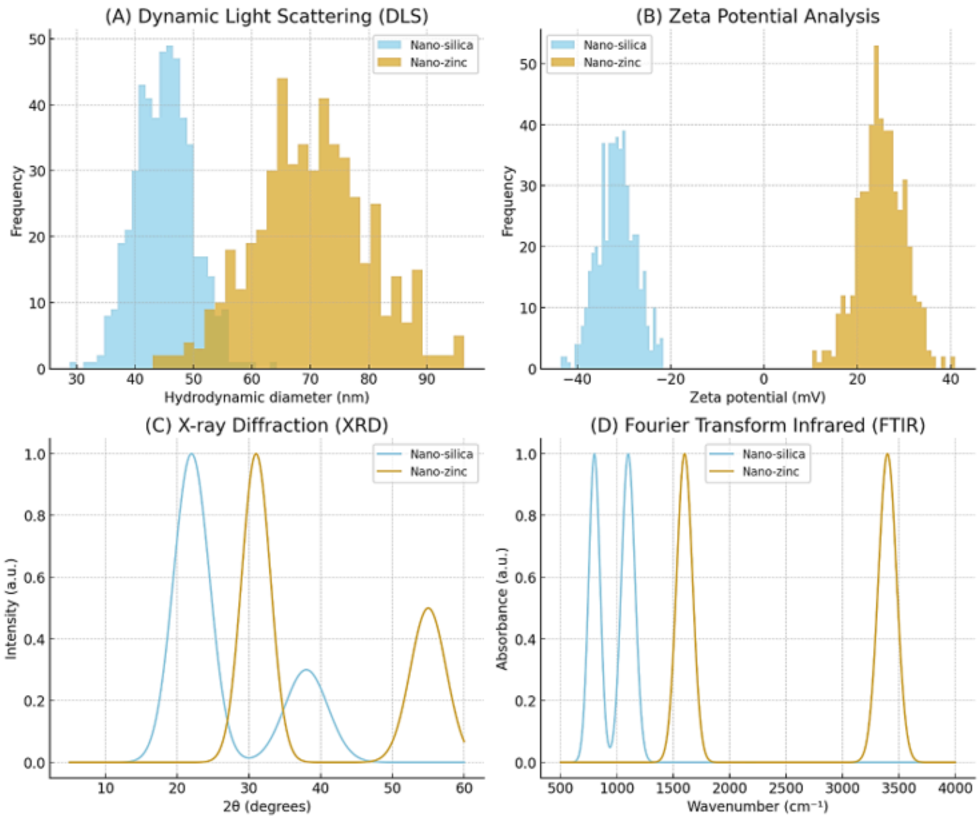

Figure 1

Physicochemical characterization of synthesized nano-silica and nano-zinc. (A) Dynamic light scattering (DLS) analysis of hydrodynamic diameter distribution, (B) zeta potential profiles, (C) X-ray diffraction (XRD) patterns, and (D) Fourier transform infrared (FTIR) spectra. Results confirm the nanoscale size distribution, surface charge stability, crystalline structure, and characteristic functional groups of the synthesized nanoparticles.

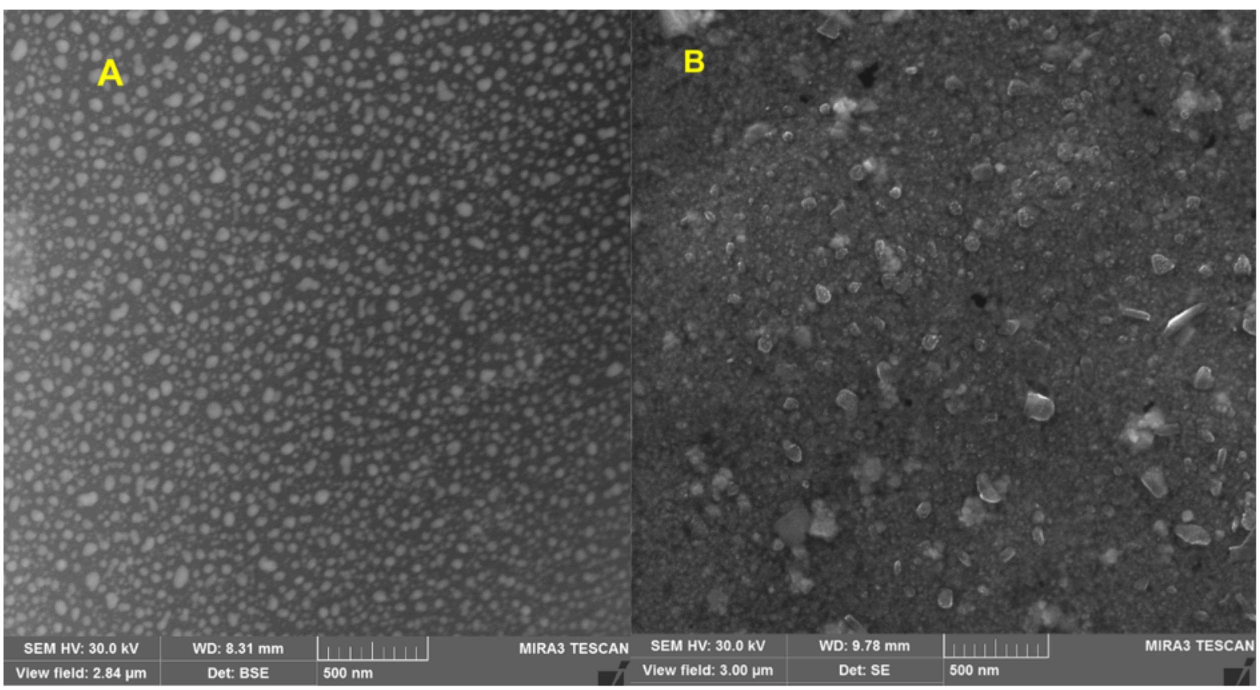

Figure 2

Scanning electron microscopy (SEM) images of synthesized nano-fertilizers. Representative micrographs showing surface morphology of (A) nano-zinc and (B) nano-silica.

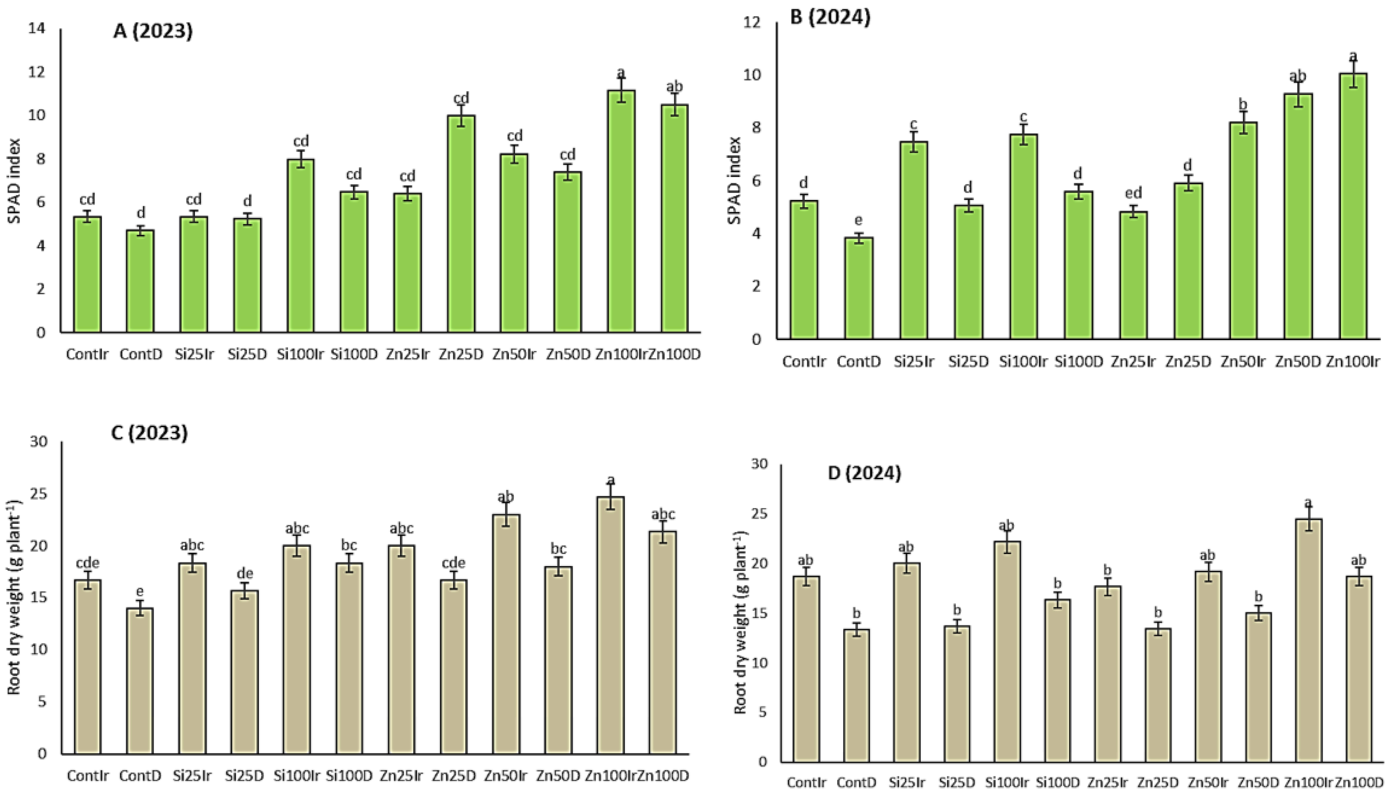

Figure 3

Effect of nano-silica and nano-zinc on SPAD index (A, B) and root dry weight (C, D) in dill (*Anethum graveolens* L.) under irrigation (Ir) and drought stress (D). Treatments included Si25 and Si100 (25 and 100 mg L^{-1} nano-silica) and Zn25, Zn50, and Zn100 (25, 50, and 100 mg L^{-1} nano-zinc) during the 2023 and 2024 seasons. Values are expressed as mean ± SE (n = 3). Different letters within a column indicate significant differences at $p < 0.05$ according to Fisher's LSD test.

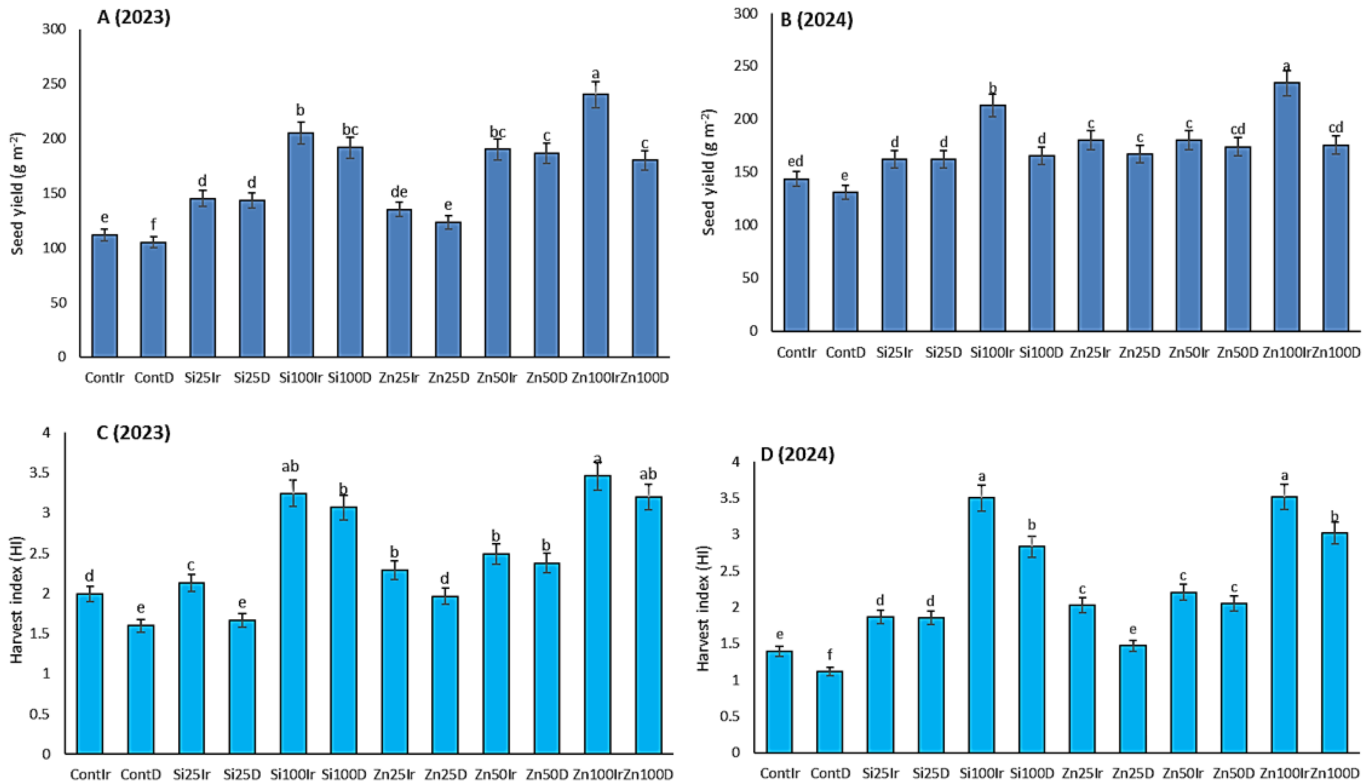

Figure 4

Effect of nano-silica and nano-zinc on seed yield (A, B) and harvest index (C, D) in dill (*Anethum graveolens* L.) under irrigation (Ir) and drought stress (D). Treatments included Si25 and Si100 (25 and 100 mg L^{-1} nano-silica) and Zn25, Zn50, and Zn100 (25, 50, and 100 mg L^{-1} nano-zinc) during the 2023 and 2024 seasons. Values are expressed as mean ± SE (n = 3). Different letters within a column indicate significant differences at $p < 0.05$ according to Fisher's LSD test.

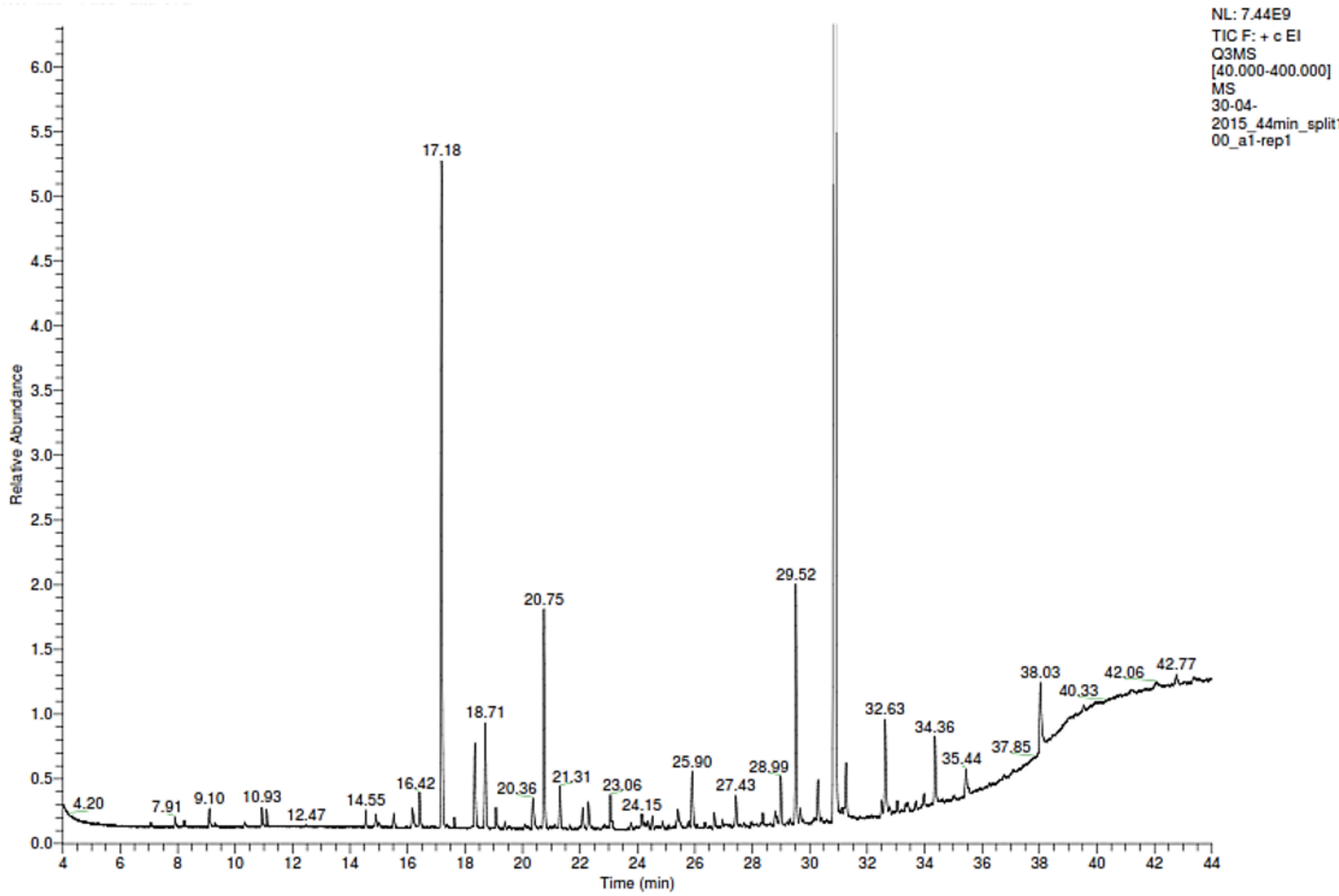

Figure 5

GC–MS chromatogram of *Anethum graveolens* essential oil. The chromatogram displays the separation profile of major volatile constituents, with peak identification corresponding to monoterpenes, oxygenated monoterpenes, and phenylpropanoid derivatives.